JOURNAL OF THERMOPHYSICS AND HEAT TRANSFER
Vol. 37, No. 2, April–June 2023

Flow and Heat Transfer from Rotating Horizontal Cylinder Floating in Stationary Fluid

Edris Torshizi* and Asghar B. Rahimi†
Ferdowsi University of Mashhad, 91775-1111 Mashhad, Iran

https://doi.org/10.2514/1.T6617

This paper investigates the flow and heat transfer from a rotating horizontal cylinder floating in a stationary fluid. The aim is to elucidate the role of angular velocity and immersion angle on heat transfer performance and fluid behavior in the flowfield. The cylinder surface has a constant temperature of 333 K, whereas the surrounding fluids are in initial thermal equilibrium at a temperature of 293 K, and the adiabatic assumption is applied to the tank walls. The results illustrate that the rotation of the cylinder causes the formation of vortices in a fluid that has a higher contact surface with the cylinder. Also, the highest-temperature gradient is observed adjacent to the surface of the cylinder. Based on the results, the creation of a liquid film on the upper surface of the cylinder exhibits a positive dependence on the angular velocity, irrespective of the immersion angle. The film thickness decreases continuously in the direction of cylinder rotation. Furthermore, increasing the immersion angle leads to an increase in the thickness and flow of the liquid film. Scrutiny of the results indicates that increasing the angular velocity and immersion angle always improves heat transfer from the surface of the cylinder.

Nomenclature

c_p	=	specific heat capacity, $J \cdot kg^{-1} \cdot K^{-1}$
D	=	cylinder diameter, m
E	=	energy, J
F_{st}	=	volume force, N
g	=	gravity acceleration, $m \cdot s^{-2}$
h	=	convective heat transfer coefficient, $W \cdot m^{-2} \cdot K^{-1}$
h_{ft}	=	liquid film thickness, m
k	=	thermal conductivity, $W \cdot m^{-1} \cdot K^{-1}$
N	=	physical property
Nu	=	Nusselt number; hD/k
n	=	surface normal gradient of ϕ
n_w	=	unit vectors normal to the wall
Pr	=	Prandtl number; $C_p\mu/k$
p	=	pressure, $N \cdot m^{-2}$
Q	=	volumetric flow rate, $m^3 \cdot s^{-1}$
R	=	cylinder radius, m
Re	=	Reynolds number; $\rho\omega R^2/\mu$
r	=	radial coordinate, m
S_e	=	source term
s	=	surface of the cylinder
T	=	temperature, K
t_w	=	unit vectors tangential to the wall
V	=	velocity, $m \cdot s^{-1}$
θ	=	angular position, deg
θ_c	=	contact angle, deg
θ_i	=	immersion angle, deg
κ	=	curvature
μ	=	viscosity, $kg \cdot m^{-1} \cdot s^{-1}$
ρ	=	density, $kg \cdot m^{-3}$
σ	=	surface tension, $N \cdot m^{-1}$
ϕ	=	volume fraction
ω	=	angular velocity, $rad \cdot s^{-1}$

Subscripts

ave	=	averaged
eff	=	effective
i	=	immersion
q	=	phase
θ	=	spatially dependent
1	=	phase 1
2	=	phase 2

I. Introduction

THE study of fluid flow and heat transfer characteristics from a cylinder has always been the goal of many researchers, which originates from the wide range of its applications in industrial and engineering processes such as cooling devices and heat exchangers, lubrication systems, textile industries, painting, paper coating, glass and plastics industries, etc. [1,2]. In general, studies in this field can be classified based on different aspects such as the flow regime (laminar or turbulent), type of fluid (Newtonian or non-Newtonian), heat transfer mechanism (natural, forced, or mixed convection), geometric configuration of the cylinder, and flow domain (bounded or unbounded) [3–6].

In a significant number of these studies, a stationary cylinder is surrounded by a quiescent fluid or exposed to a passing flow. One of the first studies concerning the heat transfer from cylinders was conducted by Tetsu and Haruo [7]. They used the perturbation method to propose separate relations for calculating the local Nusselt number along the cylinder surface in terms of that on a flat plate for conditions of constant heat flux and constant temperature. Also, Ahmad [8] analyzed the forced convection from a stationary horizontal cylinder exposed to air crossflow by solving the two-dimensional energy and Navier–Stokes equations. This work was performed in the range of the Reynolds numbers from 100 to 500, and it suggested correlations to determine the Nusselt number, drag coefficient, and separation angle in terms of the Reynolds number. In a numerical study, the free convection in an inclined enclosure with an isothermal cylinder was investigated by Park et al. [9]. Their results indicated the influence of the Rayleigh number, cylinder radius, and enclosure tilted angle on the streamlines and temperature distributions as well as the Nusselt number. In similar studies, the two-dimensional simulation of Zhang et al. [10] and the three-dimensional simulation of Souayeh et al. [11] have confirmed the same results. In other research, Taghizadeh and Asaditaheri [12] numerically analyzed the heat exchange and entropy generation in an inclined lid-driven enclosure including a porous cylinder

Received 3 April 2022; revision received 6 August 2022; accepted for publication 21 August 2022; published online 7 September 2022.

*Ph.D. Candidate, Department of Engineering.
†Professor, Department of Engineering; rahimiab@yahoo.com (Corresponding Author).

at its center. The results showed that at high Richardson numbers, the inclination angle has a more pronounced effect on the entropy generation and mixed convection. Other studies in this field have been accomplished with the presence of nanofluids (Karbasifar et al. [13]) and with two-sided lid-driven studies (Hammami et al. [14]). In an experimental study, the natural convection from a cylinder enclosed in the corner of two orthogonal adiabatic walls was examined by Sedaghat et al. [15]. Their experiments revealed that in contrast to the vertical distance between the cylinder and the walls, the horizontal distance between them and the Rayleigh number has a tangible effect on the heat transfer rate. Recently, Roy et al. [16] studied the heat transfer characteristics of flow past a heated cylinder with viscous dissipation and found that the shear stress, the point of separation, and the heat transfer rate increase with the increase of surface temperature. In addition, Maksimovich et al. [17] numerically analyzed a steady-state convective flow in the gap between two coaxial cylinders in which only half of the inner cylinder is heated. They observed that the minimum and maximum heat fluxes are observed when the heater is located in the sidewise and uppermost positions, respectively.

Reviewing the literature shows that the focus on the rotational motion of cylinders and study of its impacts on flow and heat transfer have also been considered. John et al. [18,19] compared the aerodynamic characteristics of high-speed rarefied flow past stationary and rotating cylinders and reported the impact of the rotation rate on the coefficients of drag, lift, pressure, skin friction, and heat transfer. In another comparison, the fluid mechanics and heat transfer across stationary and rotating heated cylinders were studied both numerically and experimentally by Fatla et al. [20]. Their results showed that the Nusselt number is almost independent of the Reynolds number and the thermal boundary conditions at higher rotational rates. Also, Sasmal et al. [21] numerically examined the free convection in a power-law fluid from an isothermal rotating cylinder placed at the center of a square duct. They understood that the rotation of the cylinder has an increasing impact on the heat transfer rate at low values of the Rayleigh number. In an experimental work, Ma et al. [22] investigated the role of cylinder rotation on the temperature distribution and concentration boundary layers on its surface. Their experiments proved that the temperature and concentration gradients increase continuously as the rotational Reynolds number increases. Recently, Jamal and Hussain [23] numerically analyzed the influence of a rotating cylinder inside a square cavity and iron-oxide hybrid nanofluid with water. The obtained results indicated that the averaged Nusselt number increases with the clockwise rotation of the cylinder. Furthermore, increasing the rotational speed of the cylinder enhances the local Nusselt number. Also, Thakur et al. [24] simulated the rotation of an isothermal cylinder immersed in a power-law fluid confined between two parallel walls. They found that the heat transfer rate is positively dependent on the Reynolds number and Prandtl number, as well as the confinement and degree of asymmetry.

As can be gleaned from reviewing the literature, many studies in this field have focused on stationary or rotating cylinders within a quiescent fluid or exposed to a passing flow. However, under certain conditions, a cylinder may float at the interface of two fluids, which have many applications in industry. To establish these conditions, in addition to the density, the cylinder size and the surface properties (such as the contact angle between the solid and liquid and the degree of hydrophilicity) play an essential role. The hydrophilicity is also a function of various factors, such as surface roughness and surface tension. To remain afloat, the cylinder must satisfy the condition of vertical force equilibrium so that the weight of the cylinder must be balanced by the total weight of the liquid that it displaces (Vella [25]). Generally, the resultant of buoyancy and gravity forces determines the immersion depth of the cylinder in a fluid. The equilibrium of floating objects under conditions where gravity is important was of concern to Rapacchietta et al. for a cylinder [26] and Rapacchietta and Neumann for a sphere [27], and it became clear that reducing the radius of an object increases the maximum density of floating. Hesla and Joseph [28] also reported similar observations for a circular disk.

In an applicable research, Ozeren et al. [29] experimented with the performance of a floating cylinder as a breakwater. Moreover, Bihs and Ong [30] confirmed the validity of their numerical model by comparing the obtained vertical wave forces on floating cylinders in free-surface waves with available experimental data. In another attempt, Chen et al. [31] simulated the wave-energy extraction by floating cylinders perpendicular to the wave propagation direction using the volume-of-fluid (VOF) method. Their results revealed that larger cylinders can extract more wave power than smaller ones. Also, due to the interaction between cylinders, the efficiency of the double cylinders is higher than two separate cylinders. Recently, Ageorges et al. [32] studied the free-surface flow behind a floating vertical cylinder experimentally and numerically for Reynolds numbers in the range of 30,000–200,000. The findings demonstrated that near the free surface, the interaction between the flow and the wall leads to a reduction in the cylinder drag and the creation of V-shaped surface wave patterns. Previously, they had evaluated the flow and air entrainment from a moving vertical floating cylinder, focusing on the drag force measurements and free-surface deformation [33].

Despite many theoretical and experimental studies on the flow and heat transfer from a cylinder, the study of a rotating cylinder floating in stationary fluid (in other words, a cylinder that rotates at the interface of two different fluids) has received less attention. In spite of the simple configuration in these problems, the fluid flow characteristics and heat transfer mechanism between the cylinder and the surrounding fluids are very complex. The rotational motion of the cylinder in floating conditions, in addition to affecting the flow pattern and heat transfer rate, may cause liquid to rise and form a thin layer of it on the upper surface of the cylinder. With the formation of a liquid film, the results experience impressive changes in the computational domain. Studies by Campanella and Cerro [34] and Campanella et al. [35] are scant attempts in this matter. They performed experimental and numerical investigations on the Newtonian [34] and non-Newtonian [35] flows over the outer surface of a rotating horizontal cylinder floating in a fluid. In each of these studies, the flow rate and liquid film thickness on the surface of the cylinder have been calculated in terms of the immersion angle. Apart from the cylinder discussion, more recently, Safarzadeh and Rahimi [36] numerically analyzed the flow and heat transfer from a rotating sphere around the vertical axis floating in a stationary fluid. Their results illustrated that by increasing the rotational speed, the shape of liquid film thrown out from the equator changes from large droplets to a jet. Furthermore, it was found that raising the immersion angle increases the averaged Nusselt number and the volumetric flow rate.

The present study deals with the numerical analysis of the flow and heat transfer in the problem of a rotating cylinder around its horizontal axis floating in a stationary Newtonian fluid. To the authors' best knowledge, the investigation of flow around a partially immersed rotating cylinder has rarely been the subject of a numerical simulation. In addition, no research has been found that surveyed the heat transfer from such a problem. Here, the focus is on identifying the impact of the rotation speed of the cylinder and its immersion depth on fluid flow characteristics and heat transfer performance. To that end, the contour plots of streamlines, temperatures, and volume fractions, as well as the averaged Nusselt number, liquid film thickness, and volumetric flow rate, are evaluated and compared.

II. Problem Statement and Mathematical Formulation

A. Geometric Configuration

The schematic of the present problem is depicted in Fig. 1. As can be seen, the geometry in question is a fixed cylinder with radius R and infinite length that is submerged horizontally to a certain extent in a tank of water; and its upper surface is in contact with air. The dimensions of the open tank along the x and y coordinate axes are $8R$ and $4R$, respectively and the cylinder is located at a distance of $2R$ from the tank floor. The angle between the x axis and a line connecting the center of the cylinder to the intersection point of the gas–liquid interface with the cylinder surface is the immersion angle, which is denoted in the figure by θ_i. This angle indicates the immersion depth of the cylinder in water, which is determined by the resultant of the buoyancy and gravity forces in the y direction. The floating cylinder rotates around its axis (z direction) in a counterclockwise direction with a constant angular velocity ω. The rotation of the cylinder may

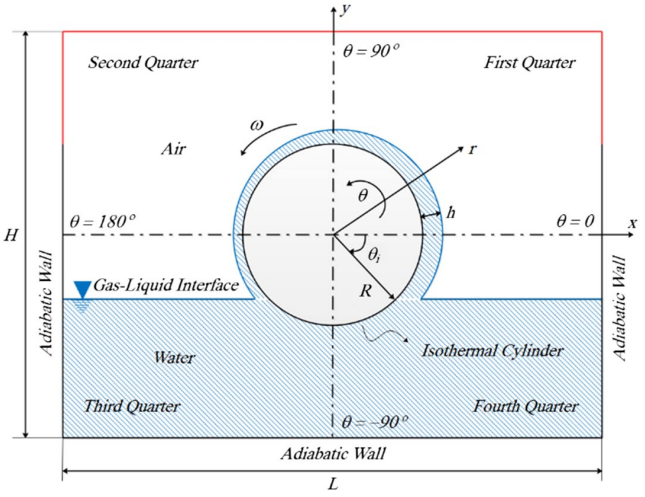

Fig. 1 Schematic geometry of the rotating horizontal cylinder floating in a stationary fluid.

cause the formation of liquid film on the cylinder with thickness h, which varies with the angular position. According to Fig. 1, the computational domain is bounded by a concentric rectangle with dimensions of $L = 8R$ and $H = 6R$, which are divided into four distinct regions from the first quarter to the fourth quarter in the positive θ direction.

B. Governing Equations

The volume-of-fluid multiphase model has been used to simulate and analyze the present problem. This model is generally a technique of transient surface tracking for two or more immiscible fluids applied to a fixed Eulerian grid in which the interface position between the fluids is of interest. In the volume-of-fluid method, the impacts of surface tension are considered, and the tracking of the interface is performed by solving a continuity equation for the volume fraction of each phase. Also, in this model, a single set of momentum and energy equations are implicitly solved, and the calculated velocity field is shared among the phases (Hirt and Nichols [37]). Based on the volume-of-fluid multiphase approach, the governing equations of the fluid flow are expressed as follows:

Continuity equation [37]:

$$\nabla \cdot V = 0 \tag{1}$$

The summation of the volume fractions for each control volume is equal to unity [37]:

$$\sum_{q=1}^{n} \phi_q = 1 \tag{2}$$

The value of ϕ_q (volume fraction of qth fluid) depends on the cell condition so that $\phi_q = 0$ when the cell is empty of the qth fluid, $\phi_q = 1$ when the cell is full of the qth fluid, and $0 < \phi_q < 1$ when the cell is partially occupied by the qth fluid.

Here, all physical properties such as viscosity and density are calculated by taking the weighted average of different phases based on their volume fractions in each control volume [37]:

$$N = \sum_{q=1}^{m} \phi_q N_q \tag{3}$$

where N represents the physical property, and m is the number of the phases.

Momentum equation [37]:

$$\nabla \cdot (\rho VV) = -\nabla p + \mu \nabla^2 V + \rho g + F_{\text{st}} \tag{4}$$

In this equation, the gravity, pressure, shear, and additional surface tension forces are balanced by the convective momentum terms and accumulated in each cell. According to Eq. (3), the density and viscosity are shared by the phases and computed as follows:

$$\rho = \phi_1 \rho_1 + \phi_2 \rho_2 \tag{5}$$

$$\mu = \phi_1 \mu_1 + \phi_2 \mu_2 \tag{6}$$

At the interface of fluids, the volume force due to the surface tension F_{st} is obtained from (Du et al. [38])

$$F_{\text{st}} = \sigma_{12} \frac{2\rho\kappa_1 \nabla \phi_1}{(\rho_1 + \rho_2)} \tag{7}$$

where κ is the surface curvature:

$$\kappa = \nabla \cdot \left(\frac{n}{|n|} \right) \tag{8}$$

and n is the surface normal gradient of ϕ.

Here, the continuum surface force model suggested by Brackbill et al. [39] is employed to estimate the surface tension, which can be expressed as the pressure jump along the surface. The pressure jump depends on the surface tension coefficient as well as the surface curvature, which is calculated by two radii in the orthogonal directions [39]:

$$p_1 - p_2 = \sigma \left(\frac{1}{R_1} + \frac{1}{R_2} \right) \tag{9}$$

Moreover, the wall adhesion effect is expressed by the following relation [39]:

$$\hat{n} = \hat{t}_w \sin\theta_c + \hat{n}_w \cos\theta_c \tag{10}$$

where $\hat{t}_w$ and $\hat{n}_w$ are the unit vectors tangential and normal to the wall, respectively; and θ_c is the contact angle at the wall.

Energy equation [37]:

$$\nabla \cdot [V(\rho E + p)] = \nabla \cdot (k_{\text{eff}} \nabla T) + S_e \tag{11}$$

In this relation, S_e is the source term that contains contributions from radiation, as well as any other volumetric heat sources. According to Eq. (3), the density and effective thermal conductivity are shared by the phases and computed as follows:

$$\rho = \phi_1 \rho_1 + \phi_2 \rho_2 \tag{12}$$

$$k_{\text{eff}} = \phi_1 k_1 + \phi_2 k_2 \tag{13}$$

The current multiphase model treats the temperature and energy as mass-averaged variables [37]:

$$E = \frac{\sum_{q=1}^{n} \phi_q \rho_q E_q}{\sum_{q=1}^{n} \phi_q \rho_q} \tag{14}$$

For each phase, E_q is based on the shared temperature and the specific heat of that phase.

The dimensionless numbers, including the Reynolds and Prandtl numbers, are defined as follows [36]:

$$Re = \frac{\rho \omega R^2}{\mu} \tag{15}$$

$$Pr = \frac{c_p \mu}{k} \tag{16}$$

After converging the computational iterations, the local and the averaged Nusselt numbers are obtained from the following equations, respectively [36]:

$$Nu_\theta = \frac{h_\theta D}{k} \tag{17}$$

$$Nu_{\text{ave}} = \frac{h_{\text{ave}} D}{k} \tag{18}$$

wherein

$$h_{\text{ave}} = \frac{1}{s}\int_s h_\theta \, \mathrm{d}s \tag{19}$$

C. Boundary Conditions

In this problem, the working fluids are assumed to be Newtonian, incompressible, quiescent, immiscible, and temperature independent. Here, the Reynolds number is much less than 8.2×10^{-6}, and therefore the flow is considered to be laminar (Johnson [40]). The air and water around the cylinder are in initial thermal equilibrium at the temperature of 293 K. Table 1 shows the thermophysical properties of the fluids at this temperature (Zahmatkesh and Torshizi [41]). In this simulation, the effects of surface tension (as well as wall adhesion) are considered, and the contact angle between water and solid surfaces is always assumed to be 90 deg. The parameters studied in this work are the angular velocity of the cylinder and the immersion angle of it, which vary from 1000 to 3000 rpm and −90 to +90 deg, respectively. As shown in Fig. 1, the cylinder surface has a constant temperature of 333 K along its circumference. The cylinder is fixed in place and does not displace with rotation. In addition, the adiabatic assumption is applied to the tank walls, and the nonslip condition is established on all solid surfaces. The boundary conditions in this problem are completed by determining the fully developed temperature profile and zero-gauge pressure at the upper boundary of the computational domain.

D. Solution Procedure

In the problem at hand, the finite volume technique is employed to discretize the governing equations (Patankar [42]). Accordingly, the computational domain is divided into distinct control volumes. Then, the partial differential governing equations are integrated over each control volume to be converted into an algebraic equations system. Finally, the obtained algebraic equations are solved iteratively through a line-by-line calculation algorithm. To solve the momentum and energy equations, a second-order upwind scheme is adopted. Moreover, for the velocity–pressure coupling, the pressure implicit with splitting of operators (PISO) method is used, which is based on the higher degree of the approximate relation between the corrections for velocity and pressure (Cheng et al. [43]). The PISO algorithm carries out two additional modifications known as neighbor and skewness corrections. In this method, the repeated calculations are transferred inside the solution stage of the pressure-correction equation (Issa [44]). Thereby, the corrected velocities satisfy the momentum and continuity equations more closely after more additional PISO loops. Besides this, after the initial solution of the pressure-correction equation, the mass flux corrections are updated by recomputing the pressure-correction gradient (Ferziger and Peric [45]). Due to the complex source terms in the momentum and energy equations, under-relaxation of the equations is implemented to ensure the stability of the numerical solution. The solution procedure is continued to satisfy the iteration convergence criterion that in all of the computations is set to be 10^{-7}.

Table 1 Thermophysical properties of the fluids at the temperature of 293 K [36,41]

Physical property	ρ, kg · m^{-3}	c_p, J · kg^{-1} · K^{-1}	k, W · m^{-1} · K^{-1}	μ, kg · m^{-1} · s^{-1}	σ, N · m^{-1}
Water	997.1	4179	0.613	0.001003	0.073
Air	1.225	1006.43	0.0242	0.00001789	

E. Grid and Domain Independence Studies

To find the appropriate size of the computational domain and grid structure, resolution tests are accomplished for the angular velocity of 2000 rpm and the immersion angle of zero. First, the calculations are carried out for three different domain sizes, and the results in terms of the average Nusselt number are reported and compared in Table 2. Based on the table, a computational domain with the size of $L \times H = 8R \times 6R$ is suitable; and increasing the domain size by a factor of 1.5 changes the averaged Nusselt number by less than 1.5%.

In the present simulation, a structured nonuniform mesh is used, which is more concentrated in the vicinity of the cylinder surface and regions close to the interface. Here, the calculations are repeated for four different grid sizes, and the results in terms of the liquid film thickness are plotted in Fig. 2. The figure clearly points out that a grid with 38,717 nodes optimizes the accuracy and cost of computations and increasing the mesh density to 59,021 nodes does not have a significant effect on the results.

Further investigations confirm the appropriateness of these values in all other circumstances as well.

F. Validation Study

To ensure the validity of the current numerical approach to describe the flow and heat transfer in this problem, the flow on the surface of a rotating horizontal cylinder floating in a stationary fluid is numerically analyzed first. Here, the cylinder with a radius of 8.47 cm and a length of 30 cm rotates with the angular velocity of 102.8 rpm at the immersion angle of 45 deg. The accuracy of the simulation is proved by comparing the results obtained from the present numerical solution with the analytical data of Campanella and Cerro [34] in Table 3. It is evident that the maximum deviation in estimating the dimensionless thickness of the liquid film on the cylinder does not exceed 4%.

For further validation and by considering the absence of any numerical or experimental data about heat transfer in the present flow problem, the validation process is performed in another fluid flow with similar conditions. In this regard, heat transfer from a rotating cylinder immersed in a power-law fluid that is asymmetrically enclosed between two parallel walls is simulated using the present numerical model.

Here, the dimensionless numbers (including the Reynolds and Prandtl numbers) as well as the blockage ratio, the power-law index, and the asymmetry ratio (eccentricity) are 40, 100, 0.9, 0.2, and 0.1,

Table 2 Domain independence study for the current problem

Domain dimensions ($L \times H$)	No. of grid nodes	Nu_{ave}	Deviation, %
$6R \times 4R$	59,021	337.978	0
$8R \times 6R$	59,021	314.045	7.08
$12R \times 9R$	59,021	309.628	1.41

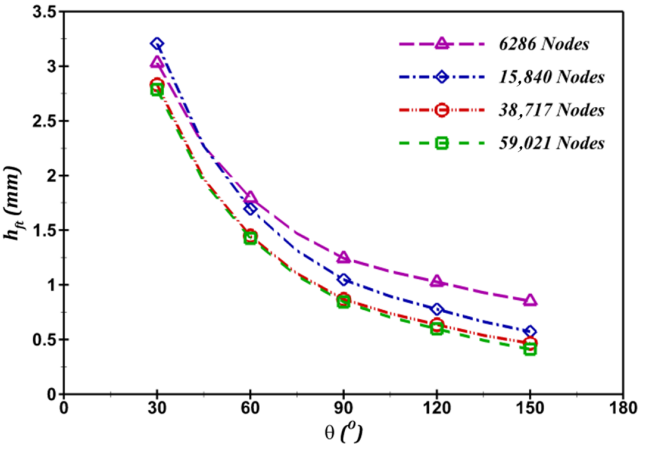

Fig. 2 Grid independence study for the current problem in terms of the spatial variation of the liquid film thickness on the cylinder surface.

Table 3 Comparing the results of present numerical solution with analytical data of Campanella and Cerro [34] in terms of dimensionless thickness of liquid film on cylinder surface at different angular positions

Angular position, deg	Present numerical solution	Campanella and Cerro [34]	Deviation, %
60	1.2590	1.2121	3.87
90	0.8228	0.8087	1.74
120	0.7451	0.7384	0.91
150	0.6632	0.6745	−1.68
180	0.5975	0.6153	−2.89

respectively. Also, the temperatures of the cylinder surface and the channel walls are constant, and the temperature difference between them is assumed to be 1 K. The obtained results are compared with those of Thakur et al. [24] in Fig. 3, which shows the local Nusselt number on the cylinder surface. It is observed that the current solution results are consistent with the data of Thakur et al. in a wide range of angular positions.

III. Results and Discussions

In this section, simulation results for the present problem, depicted in Fig. 1, are presented and discussed. The current results include contour plots of streamlines (which are colored by velocity magnitude), temperature, and volume fraction, as well as the averaged Nusselt number, liquid film thickness, and volumetric flow rate on the cylinder surface. All results are provided after 15 complete rotations of the cylinder to ensure that the steady-state solution is reached.

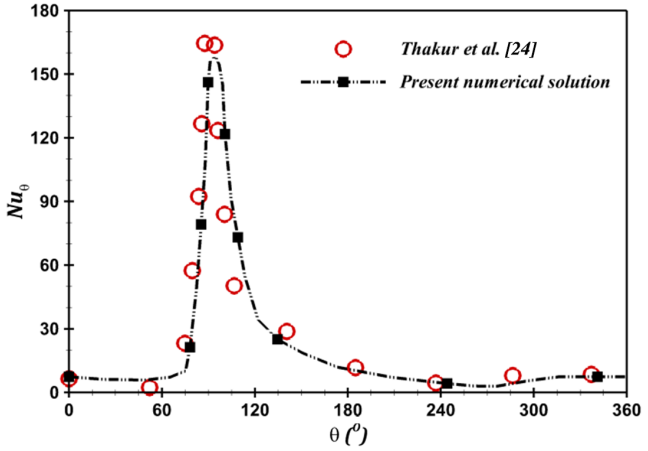

Fig. 3 Comparing the results of the present numerical solution with those of Thakur et al. [24] in terms of the local Nusselt number on the cylinder surface.

To investigate the consequence of relevant parameters on heat transfer and flow characteristics, the results are presented in two separate subsections, including the study of the effect of angular velocity and immersion angle. Before that, computations are undertaken for a base case in which the angular velocity is 2000 rpm and the immersion angle is 0 deg. The contour plots of streamlines, temperatures, and volume fractions are depicted in Fig. 4 for this case.

The streamlines in the region above the cylinder indicate an almost uniform pattern of ambient air suction that is affected by the direction of cylinder rotation; whereas the streamlines in the region below the cylinder exhibit two completely different patterns so that creating upward reverse flow in the third quarter and a giant vortex in the fourth quarter is evident. This vortex generates a huge recirculation zone in the opposite direction of the cylinder motion that causes a reverse flow at the bottom of the computational domain. Naturally, the liquid film moves faster in the second and third quarters, which is also indicated by the color of the streamlines.

Observation of the temperature contour plot in Fig. 4 illustrates that most of the temperature gradient occurs near the surface of the cylinder. The fluid around the cylinder is heated by the high temperature of its surface. Nevertheless, due to the higher heat capacity of water as compared to air, the increase in water temperature is less than air, and only a thin layer of water adjacent to the cylinder undergoes temperature changes. Therefore, despite the equality of the temperature of water and air at the initial conditions, thermal nonequilibrium arises between them. It is noteworthy that in the second and (especially) third quarters, the temperature rise is more significant in adjacent fluids. This can be attributed to the reduction of the liquid film thickness on the cylinder, and thus greater heat exchange between the cylinder surface, the thin film of water, and the surrounding air.

The last contour plot in Fig. 4 displays the water volume fraction, which provides a better view of the water–air interface and the distribution of the liquid film on the cylinder surface. As can be seen, due to the rotation of the cylinder, water rises, and a liquid film is composed on the upper surface of the cylinder. Under steady-state conditions, a uniform pattern of liquid film thickness variation is formed so that the film thickness decreases in the direction of cylinder rotation with a relatively constant slope. In addition, the interface between water and air is almost flat on the side where the liquid rises ($\theta = 0$ deg). However, on the opposite side, where the liquid film hits the water surface, unevenness is emergent in the form of waves on the interface. It is worth noting that during problem solving, tiny air bubbles emerge in the vicinity of the submerged surface of the cylinder but disappear by continuing the solution and reaching steady-state conditions.

A. Effect of the Angular Velocity

Here, the influence of the angular velocity on the flow and heat transfer characteristics is investigated. For this purpose, computations at the base case are repeated here for different values of the cylinder velocity in the range of 1000 to 3000 rpm, and the relevant results are presented. The contour plots of the streamlines, temperatures, and

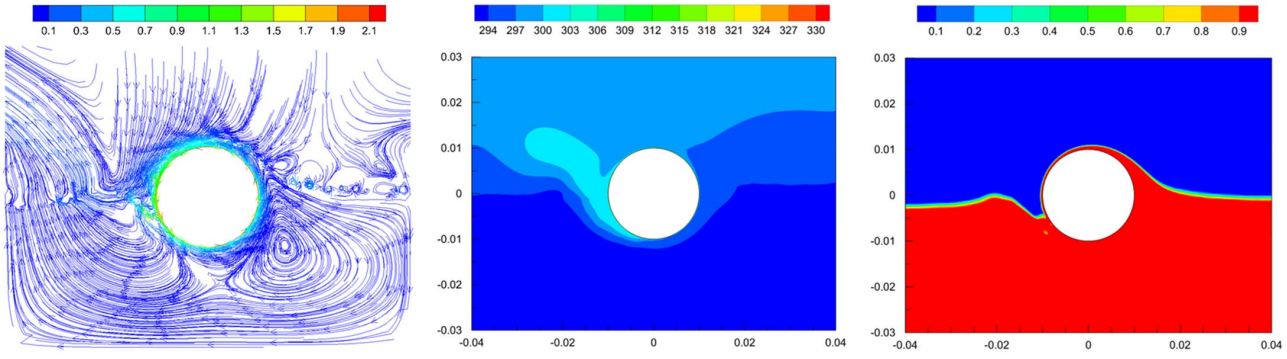

a) Streamline distribution **b) Temperature distribution** **c) Volume fraction distribution**

Fig. 4 Contour plots for the base case ($\omega = 2000$ rpm and $\theta_i = 0$ deg) at steady-state conditions.

volume fractions are shown in Fig. 5, which are comparable to the corresponding contours in Fig. 4.

At first glance, similar to the base case, the streamlines in Fig. 5 represent air suction in the region above the cylinder and the formation of a clockwise vortex in the fourth quarter. However, there are significant differences. At the lowest angular velocity ($\omega = 1000$ rpm), air suction is accompanied by the creation of vortices in the first and second quarters, which rotate in the same and opposite directions of the cylinder motion, respectively. These vortices, which can only be seen together in this case, disappear as the angular velocity increases. Another important point is the characteristics of recirculation zones and reverse flow in the water bed. Comparing the streamlines of different velocities in Fig. 5 indicates that at intermediate angular velocities, the center of the vortex formed in the fourth quarter is closer to the cylinder surface. Nevertheless, decreasing the angular velocity to 1000 rpm or increasing it to 3000 rpm leads to the formation of a vortex with a center farther from the cylinder. Despite the presence of this vortex,

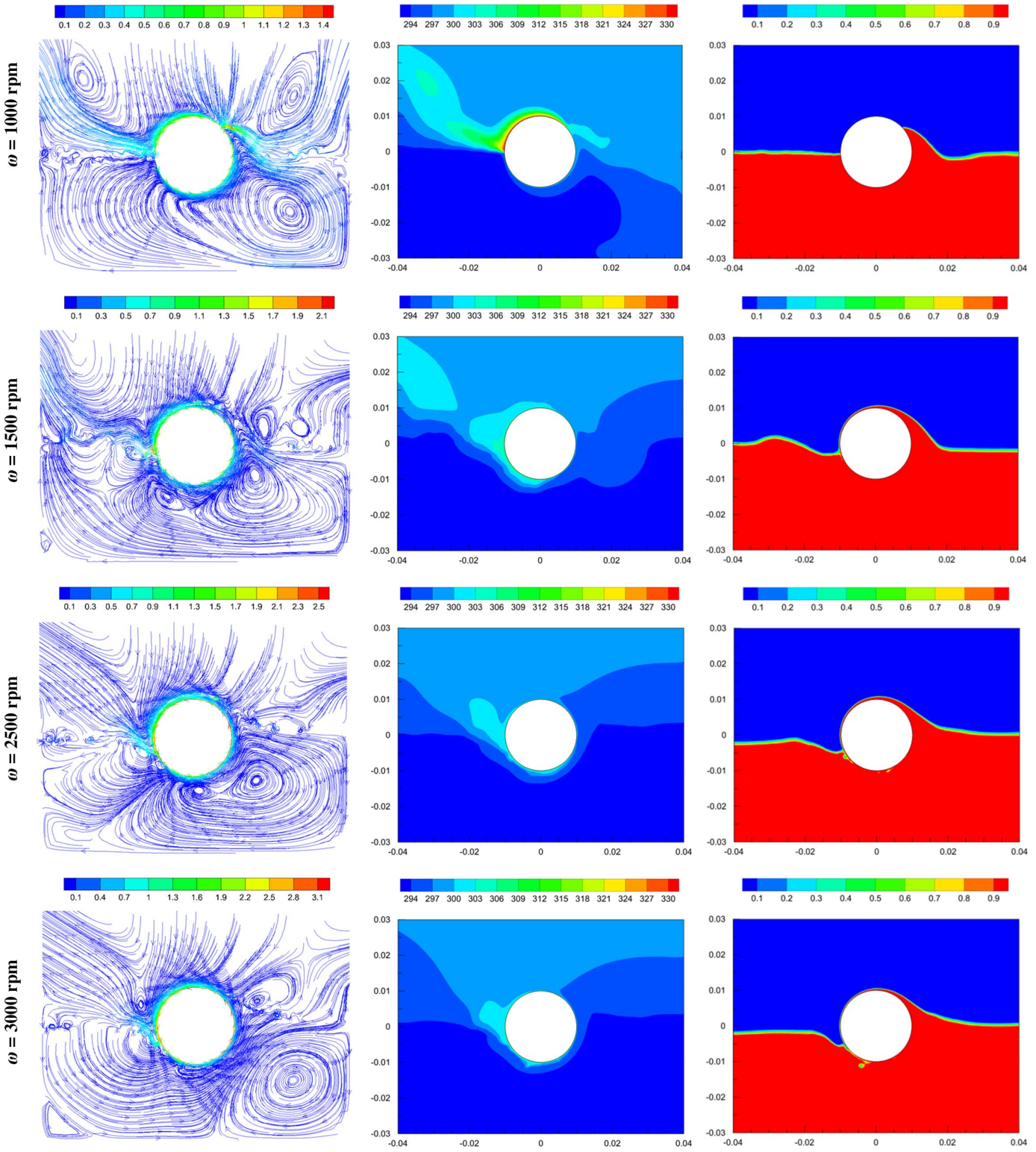

Fig. 5 Contour plots for different angular velocities at $\theta_i = 0$ deg and steady-state conditions.

which is the main cause of reverse flow in water, increasing the angular velocity prevents the spread of reverse fluid flow. At the angular velocity of 2500 rpm, the collision of the reverse flow with the direct one can be observed in the third quarter. However, the culmination of this phenomenon is seen at the angular velocity of 3000 rpm. At this velocity, the fluid flow is created precisely in the direction of the cylinder rotation in the third quarter, which originates from the high velocity of the cylinder.

Examination of the temperature distributions in Fig. 5 shows that, similar to that of the base case, most of the temperature change takes place near the cylinder surface. At the angular velocity of 1000 rpm, a faster increase in temperature occurs in adjacent fluids, which is evident for air and water in the second and fourth quarters, respectively. The noticeable increase in air temperature, in this case, can be attributed to the direct and unmediated relationship between air and the cylinder surface. However, with a rise in the angular velocity, more stability is observed in the temperature of the fluids in the flowfield. In all cases, the lowest-temperature variation is related to the water in the third quarter, which emanates from less fluid mobility in those areas.

The contour plots of the water volume fraction in Fig. 5 provide a clear picture of the impact of the angular velocity on the results. It is observed that at the angular velocity of 1000 rpm (and naturally at lower velocities), the force required to raise the water is not provided; and a part of the cylinder surface is in direct contact with air. By increasing the angular velocity, not only is it possible to form a liquid film on top of the cylinder but water harvesting is also done with a gentle slope at $\theta = 0$ deg.

The variation of the liquid film thickness on the cylinder surface versus angular position is plotted in Fig. 6 for different angular velocities. Based on the curves of this figure, there is no clear and logical relationship between the angular velocity and the thickness of the liquid film. At the angular velocity of 1000 rpm, the water rises only to an angle of about 45 deg, whereas the liquid film surrounds the cylinder as the velocity increases. On average, the maximum thickness of the liquid film is achieved at the angular velocity of 2000 rpm. Another important point in this figure is that as the angular velocity increases, the thickness of the liquid film along the angular position decreases with a gentler slope, which can also be seen in the volume fraction distributions in Fig. 5.

To investigate the effect of the angular velocity on heat transfer performance, variations of the averaged Nusselt number on the cylinder surface in terms of the immersion angle are presented in Fig. 7. In the first place, it is found that increasing the angular velocity always improves the heat exchange from the cylinder surface. This is in accord with the previous observations of Safarzadeh and Rahimi [36] in the rotating sphere problem. At the immersion angle of zero, doubling the velocity from 1500 to 3000 rpm increases the averaged Nusselt number by 48.46%. This value reaches 55.76 and 86.71% at the immersion angles of −60 and +60 deg, respectively. Exploration

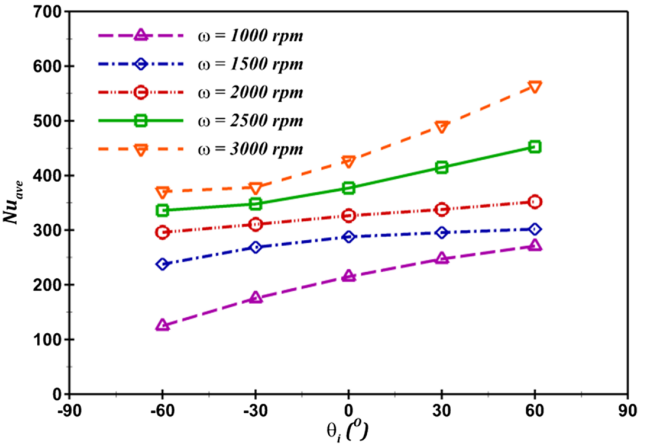

Fig. 7 Effect of the angular velocity on the averaged Nusselt number of the cylinder surface in terms of the immersion angle.

of this figure represents that at different angular velocities, the variation of the averaged Nusselt number with the immersion angle can be assumed to be almost linear. Here too, the angular velocity shows its effect so that at the minimum and maximum angular velocities, changes in the averaged Nusselt number are accompanied by a greater slope.

Figure 8 demonstrates the volumetric flow rate of water passing through a section perpendicular to the upper surface of the cylinder ($\theta = 90$ deg) as a function of immersion angle for different angular velocities.

As expected, increasing the angular velocity raises the water flow at this section. However, there is an exception in the figure that indicates a decrease in flow rate at an angular velocity of 3000 rpm. It is clear that the flow rate through each section of the cylinder depends on the angular velocity and the liquid film thickness in that section. Excessive velocity leads to the release and dispersion of liquid droplets, which reduce the thickness of the liquid film and ultimately decrease the flow rate on the cylinder. In addition, at negative immersion angles, no water flow is observed at the desired section by reducing the angular velocity to 1000 rpm or less.

B. Effect of the Immersion Angle

Another important and influential parameter on the flow and heat transfer characteristics is the immersion angle of the cylinder. To study this issue, computations at the base case are repeated here for different values of the immersion angle in the range of −90 to +90 deg, and the corresponding results are provided. In the first step, Fig. 9 presents the contour plots of streamlines, temperatures, and volume fractions that can be compared with those in Fig. 4.

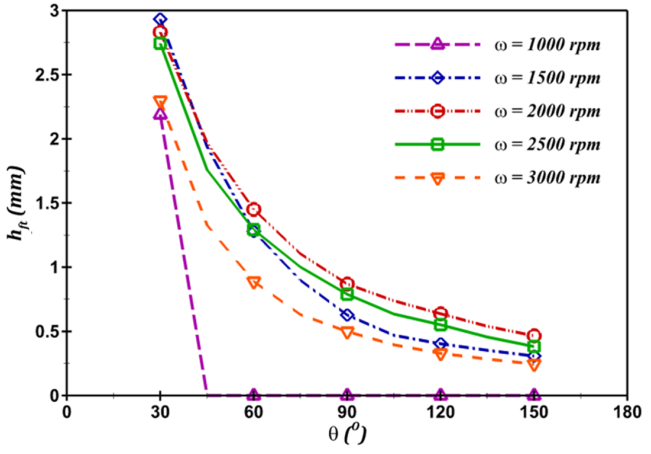

Fig. 6 Effect of the angular velocity on the spatial variation of the liquid film thickness at $\theta_i = 0$ deg.

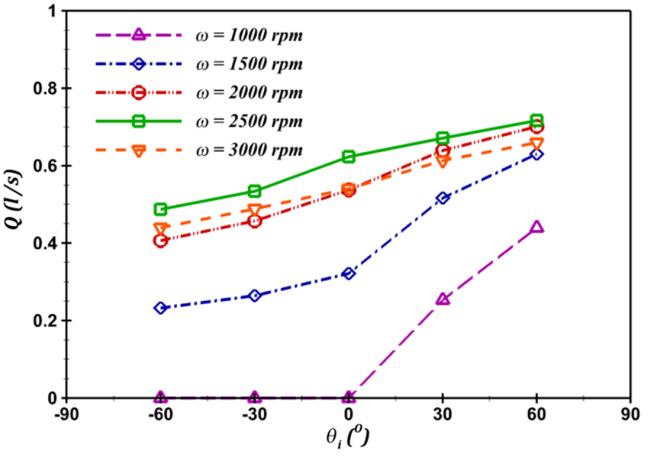

Fig. 8 Effect of the angular velocity on the volumetric flow rate of the water at $\theta = 90$ deg in terms of the immersion angle.

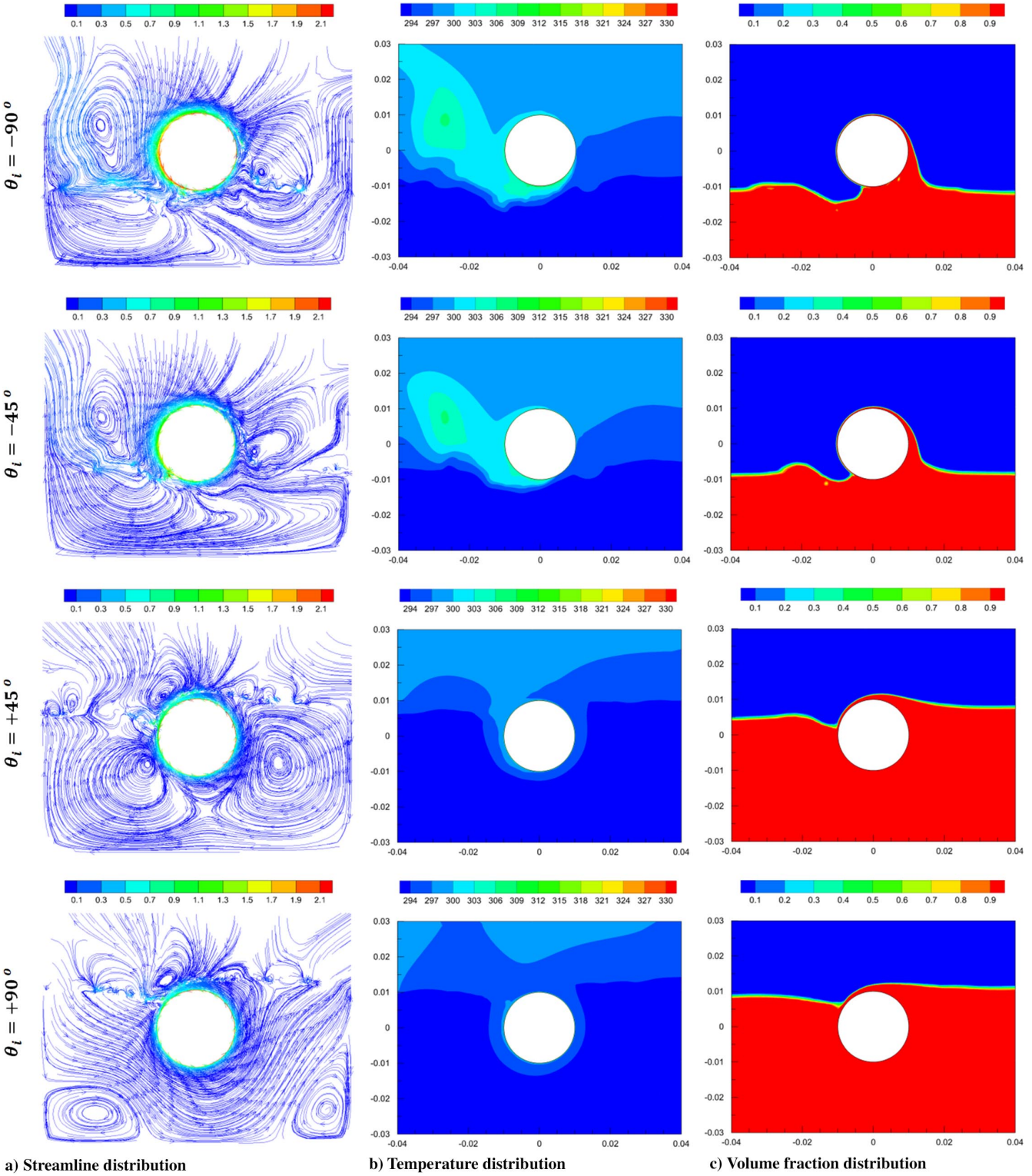

Fig. 9 Contour plots for different immersion angles at $\omega = 2000$ rpm and steady-state conditions.

Inspection of the streamlines in this figure exhibits that at an immersion angle of −90 deg, where the cylinder and water have the lowest contact surface, a wide recirculation zone appears in the air adjacent to the cylinder in the second quarter. This large vortex, which rotates in the opposite direction of the cylinder motion, takes on a vertical shape due to the low water level and the elongation along the cylinder circumference. The color spectrum of this vortex also indicates the velocity asymmetry in it. In the region below the cylinder, two different and vortex-free patterns of water flow are seen, which is in the direction of the cylinder motion in the fourth quarter and vice versa in the third one. When the water level stands at an angle of −45 deg, changes occur in the streamlines pattern, including shrinkage of the air vortex in the second quarter and codirectional water flow in the third and fourth quarters in the opposite direction of the cylinder motion. According to the contour of streamlines in Fig. 4, the water level standing in the middle of the cylinder (base case) coincides with the appearance of the water vortex in the fourth quarter. Increasing the immersion depth of the cylinder and standing the water level at an angle of +45 deg causes the simultaneous emergence of two large vortices with clockwise rotation in the water bed, which creates large recirculation zones in the opposite direction of the cylinder, especially in the fourth quarter. When the cylinder is com-

pletely submerged in water and its upper edge is in contact with the water surface ($\theta_i = +90$ deg), these vortices move away from the cylinder and transfer to the corners of the third and fourth quarters. The consequence is creation of a uniform flow in the direction of the cylinder rotation and in the form of a parabola in the water bed. Comparing the streamlines of different immersion angles in Fig. 9 proves that due to the rotation of the cylinder, vortices are generated in the fluid that has a greater contact surface with the cylinder.

Considering the temperature contours in Fig. 9 and comparing them with the corresponding contours in Fig. 4 reveals that, as expected, by increasing the contact surface between the cylinder and air at lower immersion angles, a higher temperature is observed in the surrounding air. This temperature rise is more noticeable around the air vortex in the second quarter, and it reaches its peak in the center of the vortex. Another point is that temperature changes in the fluid adjacent to the cylinder are reduced as the immersion angle increases; in other words, a fluid with a more uniform temperature surrounds the cylinder surface.

Observation of the volume fraction of water at different immersion angles displays the formation of a liquid film in all cases, which arises from the equality of the angular velocities. However, the immersion angle exerts its effect on the liquid film thickness and the reconnection point of the film to the water surface. It is expected that the liquid film hit the water surface at a level equal to the immersion angle; but, for negative angles, this point is slightly higher; and for zero and positive angles, it is slightly lower. In addition, at negative immersion angles, there is more turbulence at the water surface around the reconnection region.

It seems that at higher immersion angles, a thicker film of water forms. To examine this more closely, the variation curve of the liquid film thickness on the upper surface of the cylinder for different values of the immersion angle is plotted in Fig. 10. This figure confirms that increasing the immersion angle leads to an increment in the thickness of the liquid film. At angular positions less than 90 deg, there is a significant difference between the liquid film thickness at different immersion angles. Nevertheless, as the angular position reaches 150 deg, this difference fades. To put it simply, at higher immersion angles, the liquid film thickness versus angular position decreases with a steeper slope. This behavior has also been reported by Campanella and Cerro [34] and Safarzadeh and Rahimi [36].

Figure 11 is presented to investigate the effect of the immersion angle on heat transfer performance, which shows the averaged Nusselt number values on the cylinder surface in terms of the Reynolds number. At first sight, it is clear that increasing the immersion angle promotes heat exchange between the cylinder surface and the surrounding fluids. This is also in agreement with the previous evidence of Safarzadeh and Rahimi [36] in the rotating sphere problem. At the Reynolds number of 20,000, tripling the contact surface between the cylinder and water by varying the immersion angle from −45 to +45 deg increases the averaged Nusselt number by 14.75%. These values reach 77 and 39.21% at Reynolds numbers of 10,000 and

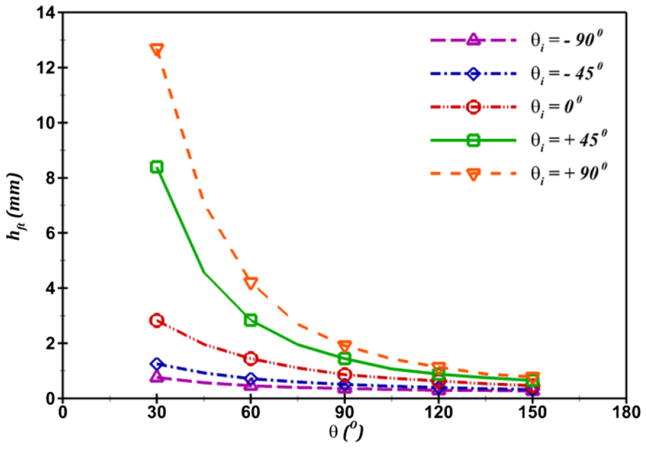

Fig. 10 Effect of the immersion angle on the spatial variation of the liquid film thickness at $\omega = 2000$ rpm.

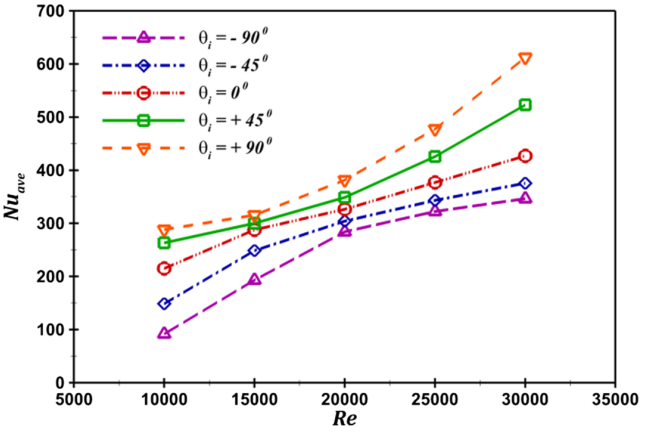

Fig. 11 Effect of the immersion angle on the averaged Nusselt number of the cylinder surface in terms of the Reynolds number.

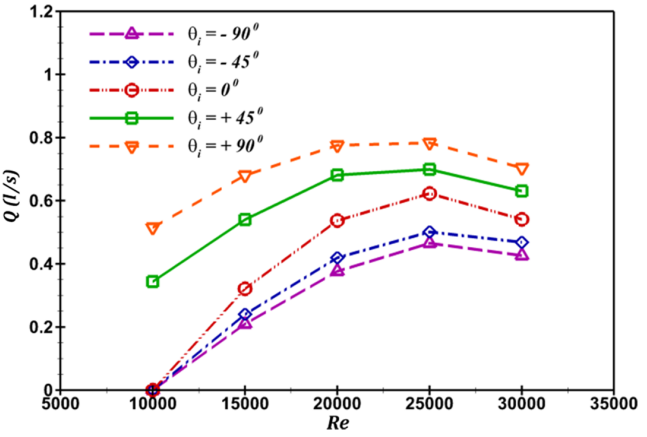

Fig. 12 Effect of the immersion angle on the volumetric flow rate of the water at $\theta = 90$ deg in terms of the Reynolds number.

30,000, respectively. Inspection of this figure demonstrates that at nonzero immersion angles, the variation curve of the averaged Nusselt number with the Reynolds number is almost parabolic. Here too, the immersion angle represents its effect so that the parabola is concave downward at negative angles and is concave upward at positive angles. Therefore, by synchronizing the negative and positive immersion angles with the low and high Reynolds numbers, respectively, the changes in the averaged Nusselt number are accompanied by a greater slope.

Figure 12 illustrates the volumetric flow rate of water passing through a section perpendicular to the upper surface of the cylinder ($\theta = 90$ deg) as a function of the Reynolds number for different immersion angles. It can be clearly seen that increasing the immersion angle leads to a higher flow rate at this section. At the same Reynolds number, the differences between the flow rates are reduced by decreasing the immersion angle. In other words, changing the immersion angle in its positive range has a more remarkable effect on the water flow rate. Examination of this figure reveals that in conditions where the water does not rise enough (the flow rate at $\theta = 90$ deg is zero), increasing the Reynolds number at any immersion angle helps to form a liquid film on the cylinder surface and to create a flow on it. In addition, exceeding the Reynolds number of 30,000 due to the increase in angular velocity causes a drop in water flow rate, and its reason has been mentioned previously.

IV. Conclusions

In the present study, a numerical analysis of flow and heat transfer in a rotating cylinder around a horizontal axis floating in a stationary fluid has been presented and discussed. Computations have been performed using a two-phase VOF model focusing on studying the

impact of two key parameters, including the angular velocity and immersion angle, and the results have been compared with each other. Based on the obtained results, the following can be concluded:

1) When the water level stands in the middle of the cylinder ($\theta_i = 0$ deg), a giant vortex is always created in the fourth quarter, which is the leading cause of reverse flow in the water bed. By increasing the angular velocity, the vortices in the air disappear, and the flow is formed in the direction of the cylinder rotation in the water bed. Moreover, by changing the immersion angle from negative to positive values, the air vortex gradually vanishes and vortices are generated in the water instead. Therefore, the rotation of the cylinder causes the formation of vortices in a fluid that has a higher contact surface with the cylinder.

2) In all cases, the highest-temperature gradient occurs near the cylinder surface, especially in the second quarter. By increasing the angular velocity and the immersion angle, a higher-temperature equilibrium prevails in the flowfield; as a result, fluids with a more uniform temperature surround the surface of the cylinder.

3) By rotating the cylinder with an appropriate velocity, it is possible to form a continuous film of liquid on the cylinder surface at any immersion angle, with its thickness decreasing uniformly in the direction of rotation. The configuration pattern of the liquid film depends on the angular velocity as well as the immersion angle, and increasing each of these parameters facilitates the formation process. In addition, by increasing the immersion angle, less turbulence and more stability are observed at the contact surface between water and air.

4) It is impossible to define a linear and precise relationship between the angular velocity and the liquid film thickness. In this problem, the maximum thickness of the water film is obtained at the angular velocity of 2000 rpm. On the other hand, increasing the immersion angle always leads to an increase in the thickness of the liquid film. It can be approximately concluded that by increasing the angular velocity and immersion angle, the decreasing slope of the liquid film thickness in terms of the angular position decreases and increases, respectively.

5) Increasing the angular velocity and the immersion angle always improves heat exchange from the cylinder surface. The simultaneous rise in the angular velocity and immersion angle increases heat transfer with greater slope. Regardless of the exceptions, the variation curve of the averaged Nusselt number in terms of the Reynolds number is approximately parabolic. The curve is concave downward and upward at negative and positive immersion angles, respectively.

6) The flow rate through each section of the cylinder depends on the angular velocity and the liquid film thickness in that section. In most cases, the higher rotational velocity of the cylinder causes an increase in water flow. However, excessive velocity leads to the release and dispersion of liquid droplets, which decrease the liquid film thickness and the water flow on the cylinder. Increasing the immersion angle always promotes the water flow rate, which is more remarkable at positive immersion angles.

References

[1] Zdravkovich, M. M., *Flow Around Circular Cylinders: Volume 1: Fundamentals*, Vol. 1, Oxford Univ. Press, Oxford, England, U.K., 1997.
https://doi.org/10.1017/s0022112097227291

[2] Khan, W. A., Culham, J. R., and Yovanovich, M. M., "Fluid Flow and Heat Transfer from a Cylinder Between Parallel Planes," *Journal of Thermophysics and Heat Transfer*, Vol. 18, No. 3, 2004, pp. 395–403.
https://doi.org/10.2514/1.6186

[3] Fetecau, C., Ellahi, R., Khan, M., and Shah, N. A., "Combined Porous and Magnetic Effects on Some Fundamental Motions of Newtonian Fluids over an Infinite Plate," *Journal of Porous Media*, Vol. 21, No. 7, 2018, pp. 589–605.
https://doi.org/10.1615/jpormedia.v21.i7.20

[4] Shehzad, N., Zeeshan, A., Shakeel, M., Ellahi, R., and Sait, S. M., "Effects of Magnetohydrodynamics Flow on Multilayer Coatings of Newtonian and Non-Newtonian Fluids Through Porous Inclined Rotating Channel," *Coatings*, Vol. 12, No. 4, 2022, p. 430.
https://doi.org/10.3390/coatings12040430

[5] Zeeshan, A., Shehzad, N., Atif, M., Ellahi, R., and Sait, S. M., "Electromagnetic Flow of SWCNT/MWCNT Suspensions in Two Immiscible Water-And Engine-Oil-Based Newtonian Fluids Through Porous Media," *Symmetry*, Vol. 14, No. 2, 2022, Paper 406.

[6] Tripathi, D., Prakash, J., Tiwari, A. K., and Ellahi, R., "Thermal, Microrotation, Electromagnetic Field and Nanoparticle Shape Effects on Cu-CuO/Blood Flow in Microvascular Vessels," *Microvascular Research*, Vol. 132, Nov. 2020, Paper 104065.
https://doi.org/10.1016/j.mvr.2020.104065

[7] Tetsu, F., and Haruo, U., "Laminar Natural-Convective Heat Transfer from the Outer Surface of a Vertical Cylinder," *International Journal of Heat and Mass Transfer*, Vol. 13, No. 3, 1970, pp. 607–615.
https://doi.org/10.1016/0017-9310(70)90155-9

[8] Ahmad, R. A., "Steady-State Numerical Solution of the Navier-Stokes and Energy Equations Around a Horizontal Cylinder at Moderate Reynolds Numbers from 100 to 500," *Heat Transfer Engineering*, Vol. 17, No. 1, 1996, pp. 31–81.
https://doi.org/10.1080/01457639608939866

[9] Park, H. K., Ha, M. Y., Yoon, H. S., Park, Y. G., and Son, C., "A Numerical Study on Natural Convection in an Inclined Square Enclosure with a Circular Cylinder," *International Journal of Heat and Mass Transfer*, Vol. 66, Nov. 2013, pp. 295–314.
https://doi.org/10.1016/j.ijheatmasstransfer.2013.07.029

[10] Zhang, P., Zhang, X., Deng, J., and Song, L., "A Numerical Study of Natural Convection in an Inclined Square Enclosure with an Elliptic Cylinder Using Variational Multiscale Element Free Galerkin Method," *International Journal of Heat and Mass Transfer*, Vol. 99, Aug. 2016, pp. 721–737.
https://doi.org/10.1016/j.ijheatmasstransfer.2016.04.011

[11] Souayeh, B., Ben-Cheikh, N., and Ben-Beya, B., "Numerical Simulation of Three-Dimensional Natural Convection in a Cubic Enclosure Induced by an Isothermally-Heated Circular Cylinder at Different Inclinations," *International Journal of Thermal Sciences*, Vol. 110, Dec. 2016, pp. 325–339.
https://doi.org/10.1016/j.ijthermalsci.2016.08.003

[12] Taghizadeh, S., and Asaditaheri, A., "Heat Transfer and Entropy Generation of Laminar Mixed Convection in an Inclined Lid Driven Enclosure with a Circular Porous Cylinder," *International Journal of Thermal Sciences*, Vol. 134, Dec. 2018, pp. 242–257.
https://doi.org/10.1016/j.ijthermalsci.2018.08.018

[13] Karbasifar, B., Akbari, M., and Toghraie, D., "Mixed Convection of Water-Aluminum Oxide Nanofluid in an Inclined Lid-Driven Cavity Containing a Hot Elliptical Centric Cylinder," *International Journal of Heat and Mass Transfer*, Vol. 116, Jan. 2018, pp. 1237–1249.
https://doi.org/10.1016/j.ijheatmasstransfer.2017.09.110

[14] Hammami, F., Souayeh, B., Ben-Cheikh, N., and Ben-Beya, B., "Computational Analysis of Fluid Flow due to a Two-Sided Lid Driven Cavity with a Circular Cylinder," *Computers and Fluids*, Vol. 156, Oct. 2017, pp. 317–328.
https://doi.org/10.1016/j.compfluid.2017.07.017

[15] Sedaghat, M. H., Yaghoubi, M., and Maghrebi, M. J., "Analysis of Natural Convection Heat Transfer from a Cylinder Enclosed in a Corner of Two Adiabatic Walls," *Experimental Thermal and Fluid Science*, Vol. 62, April 2015, pp. 9–20.
https://doi.org/10.1016/j.expthermflusci.2014.11.003

[16] Roy, N. C., Rahman, T., Hossain, M. A., and Gorla, R. S. R., "Boundary-Layer Characteristics of Compressible Flow Past a Heated Cylinder with Viscous Dissipation," *Journal of Thermophysics and Heat Transfer*, Vol. 33, No. 1, 2019, pp. 10–22.
https://doi.org/10.2514/1.t5400

[17] Maksimovich, G. M., Araratovich, S. K., Nikolaevna, B. E., and Alekseevich, O. A., "Gravity Orientation Effects on Convection in the Gap Between Partially Heated Cylinders," *Journal of Thermophysics and Heat Transfer*, Vol. 36, No. 3, 2022, pp. 1–9.
https://doi.org/10.2514/1.T6394

[18] John, B., Gu, X., Barber, R., and Emerson, D., "High Speed Aerodynamic Characteristics of Rarefied Flow Past Stationary and Rotating Cylinders," *20th AIAA International Space Planes and Hypersonic Systems and Technologies Conference*, AIAA Paper 2015-3511, 2015.
https://doi.org/10.2514/6.2015-3511

[19] John, B., Gu, X. J., Barber, R. W., and Emerson, D. R., "High-Speed Rarefied Flow past a Rotating Cylinder: The Inverse Magnus Effect," *AIAA Journal*, Vol. 54, No. 5, 2016, pp. 1670–1681.
https://doi.org/10.2514/1.j054782

[20] Fatla, O. M. H., Smaism, G. F., Valera-Medina, A., Rageb, A. M., and Syred, N., "Investigation of Heat Transfer and Fluid Mechanics Across a Heated Rotating Circular Cylinder in Crossflow," *54th AIAA Aerospace Sciences Meeting, AIAA SciTech Forum*, AIAA Paper 2016-0494, 2016.
https://doi.org/10.2514/6.2016-0494

[21] Sasmal, C., Gupta, A. K., and Chhabra, R. P., "Natural Convection Heat Transfer in a Power-Law Fluid from a Heated Rotating Cylinder in a

Square Duct," *International Journal of Heat and Mass Transfer*, Vol. 129, Feb. 2019, pp. 975–996.
https://doi.org/10.1016/j.ijheatmasstransfer.2018.10.007

[22] Ma, H., Yin, L., Zhou, W., Lv, X., Cao, Y., Shen, X., and Lu, W., "Measurement of the Temperature and Concentration Boundary Layers from a Horizontal Rotating Cylinder Surface," *International Journal of Heat and Mass Transfer*, Vol. 87, Aug. 2015, pp. 481–490.
https://doi.org/10.1016/j.ijheatmasstransfer.2015.04.035

[23] Jamal, M., and Hussain, S., "Mixed Convection in Square Enclosure by Considering the Thermal Effect on Cylinder," *Journal of Thermophysics and Heat Transfer*, Vol. 35, No. 4, 2021, pp. 869–882.
https://doi.org/10.2514/1.T6214

[24] Thakur, P., Tiwari, N., and Chhabra, R. P., "Momentum and Heat Transfer from an Asymmetrically Confined Rotating Cylinder in a Power-Law Fluid," *International Journal of Thermal Sciences*, Vol. 137, March 2019, pp. 410–430.
https://doi.org/10.1016/j.ijthermalsci.2018.11.034

[25] Vella, D. J. R., "The Fluid Mechanics of Floating and Sinking," Ph.D. Dissertation, Univ. of Cambridge, Cambridge, England, U.K., 2007.

[26] Rapacchietta, A. V., Neumann, A. W., and Omenyi, S. N., "Force and Free-Energy Analyses of Small Particles at Fluid Interfaces: I. Cylinders," *Journal of Colloid and Interface Science*, Vol. 59, No. 3, 1977, pp. 541–554.
https://doi.org/10.1016/0021-9797(77)90050-9

[27] Rapacchietta, A. V., and Neumann, A. W., "Force and Free-Energy Analyses of Small Particles at Fluid Interfaces: II. Spheres," *Journal of Colloid and Interface Science*, Vol. 59, No. 3, 1977, pp. 555–567.
https://doi.org/10.1016/0021-9797(77)90051-0

[28] Hesla, T. I., and Joseph, D. D., "The Maximum Contact Angle at the Rim of a Heavy Floating Disk," *Journal of Colloid and Interface Science*, Vol. 279, No. 1, 2004, pp. 186–191.
https://doi.org/10.1016/j.jcis.2004.06.055

[29] Ozeren, Y., Wren, D. G., Altinakar, M., and Work, P. A., "Experimental Investigation of Cylindrical Floating Breakwater Performance with Various Mooring Configurations," *Journal of Waterway, Port, Coastal, and Ocean Engineering*, Vol. 137, No. 6, 2011, pp. 300–309.
https://doi.org/10.1061/(asce)ww.1943-5460.0000090

[30] Bihs, H., and Ong, M. C., "Numerical Simulation of Flows Past Partially-Submerged Horizontal Circular Cylinders in Free Surface Waves," *International Conference on Offshore Mechanics and Arctic Engineering*, Vol. 55416, American Soc. of Mechanical Engineers, Fairfield, VA, June 2013, p. V007T08A036.
https://doi.org/10.1115/omae2013-10529

[31] Chen, B., Ning, D., Liu, C., Greated, C. A., and Kang, H., "Wave Energy Extraction by Horizontal Floating Cylinders Perpendicular to Wave Propagation," *Ocean Engineering*, Vol. 121, July 2016, pp. 112–122.
https://doi.org/10.1016/j.oceaneng.2016.05.016

[32] Ageorges, V., Peixinho, J., Perret, G., Lartigue, G., and Moureau, V., "Experiments and Simulations of Free-Surface Flow Behind a Finite Height Rigid Vertical Cylinder," *Fluids*, Vol. 6, No. 10, 2021, Paper 367.
https://doi.org/10.3390/fluids6100367

[33] Ageorges, V., Peixinho, J., and Perret, G., "Flow and Air-Entrainment Around Partially Submerged Vertical Cylinders," *Physical Review Fluids*, Vol. 4, No. 6, 2019, Paper 064801.
https://doi.org/10.1103/physrevfluids.4.064801

[34] Campanella, O. H., and Cerro, R. L., "Viscous Flow on the Outside of a Horizontal Rotating Cylinder: The Roll Coating Regime with a Single Fluid," *Chemical Engineering Science*, Vol. 39, No. 10, 1984, pp. 1443–1449.
https://doi.org/10.1016/0009-2509(84)80002-0

[35] Campanella, O. H., Galazzo, J. L., and Cerro, R. L., "Viscous Flow on the Outside of a Horizontal Rotating Cylinder—II. Dip Coating with a Non-Newtonian Fluid," *Chemical Engineering Science*, Vol. 41, No. 11, 1986, pp. 2707–2713.
https://doi.org/10.1016/0009-2509(86)80001-x

[36] Safarzadeh, S., and Rahimi, A. B., "Numerical Investigation of Flow and Heat Transfer From a Rotating Sphere with Constant Angular Velocity Around Vertical Axis Floating in Stationary Fluid," *Journal of Heat Transfer*, Vol. 144, No. 2, 2022, Paper 021802.
https://doi.org/10.1115/1.4053008

[37] Hirt, C. W., and Nichols, B. D., "Volume of Fluid (VOF) Method for the Dynamics of Free Boundaries," *Journal of Computational Physics*, Vol. 39, No. 1, 1981, pp. 201–225.
https://doi.org/10.1016/0021-9991(81)90145-5

[38] Du, W., Feng, D., Xu, J., and Wei, W., "Computational Fluid Dynamics Modeling of Gas–Liquid Two-Phase Flow Around a Spherical Particle," *Chemical Engineering and Technology*, Vol. 36, No. 5, 2013, pp. 840–850.
https://doi.org/10.1002/ceat.201200486

[39] Brackbill, J. U., Kothe, D. B., and Zemach, C., "A Continuum Method for Modeling Surface Tension," *Journal of Computational Physics*, Vol. 100, No. 2, 1992, pp. 335–354.
https://doi.org/10.1016/0021-9991(92)90240-y

[40] Johnson, N. D., "High-Reynolds Number Flow Past a Rotating Cylinder with and Without Thom Discs," Ph.D. Dissertation, Univ. of Manchester, Manchester, England, U.K., 2011.

[41] Zahmatkesh, I., and Torshizi, E., "Scrutiny of Unsteady Flow and Heat Transfer in a Backward-Facing Step Under Pulsating Nanofluid Blowing Using the Eulerian-Eulerian Approach," *Journal of Mechanics*, Vol. 35, No. 1, 2019, pp. 93–105.
https://doi.org/10.1017/jmech.2017.73

[42] Patankar, S. V., *Numerical Heat Transfer and Fluid Flow*, 1st ed., CRC Press, Boca Raton, FL, 1980.
https://doi.org/10.1201/9781482234213

[43] Cheng, X., Chen, Y., and Luo, L., "Numerical Simulation of Air-Water Two-Phase Flow over Stepped Spillways," *Science in China, Series E: Technological Sciences*, Vol. 49, No. 6, 2006, pp. 674–684.
https://doi.org/10.1007/s10288-006-2029-2

[44] Issa, R. I., "Solution of the Implicitly Discretised Fluid Flow Equations by Operator-Splitting," *Journal of Computational Physics*, Vol. 62, No. 1, 1986, pp. 40–65.
https://doi.org/10.1016/0021-9991(86)90099-9

[45] Ferziger, J. H., and Peric, M., *Computational Methods for Fluid Dynamics*, Springer-Verlag, New York, 1996.
https://doi.org/10.1007/978-3-642-97651-3